Resonant Capture of Low-Energy Electrons by Gas-Phase Glycine: A Quantum Dynamics Calculation

F. A. Gianturco

Department of Chemistry, University of Rome "La Sapienza" and INFM, Piazzale A. Moro 5, 00185 Rome, Italy

R. R. Lucchese*

Department of Chemistry, Texas A&M University, College Station, Texas 77843-3255

Received: February 19, 2004; In Final Form: June 21, 2004

We present quantum calculations for the low-energy dynamics of electrons interacting with glycine molecules in the gas phase. The scattering equations are formulated within a symmetry-adapted, single-center expansion of both continuum and bound electrons, and the interaction forces are obtained from a combination of ab initio calculations and a nonempirical modeling of exchange plus correlation effects. Several open-channel (shape) resonances are obtained, and the features of the excess electron resonant wave functions are related to the experimental findings about the dissociative electron attachment (DEA) processes that follow the initial formation of those transient negative ions.

I. Introduction

Glycine is the simplest of the α-amino acids, and therefore it has been, over the years, an important model compound in biophysics and biochemistry, providing the subject for many experimental[1−4] and theoretical[5−10] investigations. The −N−C−C−O− structure contained in glycine is an important strand of the α-amino acids and of the proteins derived from them. The studies on the possible consequences of damaging such a building block have attracted a great deal of interest in recent years, not only on glycine[11,12] but also on the more general class of DNA strands, where it has been shown that low-energy electrons with collision energy below about 15 eV can cause considerable damage through the detachment of specific molecular units[13,14] present in the oligonucleotides and in double-stranded DNA. Such damage has been found to be related to the formation of a variety of transient negative ions (TNIs) involving one of the basic units of the double strands, which can then decay into electronic excitation and/or dissociative electron attachment (DEA) channels.[15]

Even if the theoretical treatments of low-energy electron scattering processes have been fairly successful in the past 10 years or so[16] in describing a broad variety of channels in molecular systems, no suitable computational framework presently exists for treating scattering problems involving several hundreds of bound electrons which are coupled to nuclear motions within polyatomic networks with several thousand atoms in them.

In the relatively simple case of glycine one may still manage to obtain some information on its structural properties[8] and on the stable structures of its radicals and of its anions,[9,10,12] while the actual dynamical treatment of the electron scattering processes coupled to the multidimensional nuclear motion of the bound molecule still remains entirely out of reach for a full treatment of all its degrees of freedom.

We have therefore explored, in recent years, the extent to which fairly large polyatomic systems such as SF_6, C_6H_6, C_{20}, and C_{60} could be analyzed in terms of the structures of their metastable, resonant anions by employing a quantum formulation of the elastic scattering processes using a local, energy-dependent, nonempirical model potential.[17−20]

More recently, we have applied a similar analysis to the location of TNI species from low-energy electron scattering of gas-phase uracil molecules[21] and found reasonable correlation between such resonances and the DEA experiments carried out on that molecule.[22] The purpose of the present work is therefore to see if a similar procedure and computational modeling of the scattering dynamics could be applied to the glycine molecule in the gas phase and if the results could be employed to analyze the recent experimental findings[11] on this system, thereby providing a structural rationalization for the fragmentation channels found by the above measurements.[11]

To understand the recent experimental findings on the DEA processes of gas-phase glycine molecules initiated by electron impact,[11] we have studied the quantum dynamics of low-energy electrons ($E_{coll} < 15$ eV) scattered off the glycine molecule and have searched for the presence of single-particle trapped states or shape resonances which could give rise to TNI species in that range of energies. We have found four different resonant states of such temporary anions and established their energies and widths using molecular equilibrium geometries; we have examined the three lowest energy nuclear arrangements for the isolated glycine since they are all very close to each other in terms of total energies. The experiments[11] have shown that the low-energy DEA process involves eight or nine different fragmentation channels at electron energies below 8 eV and a secondary, broad peak around 12.0 eV. The most intense peak appears at low energy and gives rise to the H abstraction process leading to the a $[Gly-H]^-$ residual anion. It correlates well with our low-energy computed resonance of A″ symmetry which clearly indicates that it is a precursor state that could cause H atom release during TNI stabilization.

We know that the interaction of ionizing radiation with matter generates secondary species along the ionization tracks[13,23] and that, among the most reactive of them, the ballistic electrons

10.1021/jp049237y CCC: $27.50
Published on Web 07/31/2004

are fairly abundant, possessing kinetic energy values which peak around 15 eV. In the following dynamical evolution, these electrons undergo successive inelastic collisions and eventually thermalize, becoming solvated within about 10^{-12} s. However, the action of the presolvated, nonthermalized electrons on the surrounding biological medium is of great importance since it has been considered over the years to be the prime source of reactivity that can cause permanent damage of the biological species by their interaction with such secondary electrons before their solvation.[24] The recent DEA experiments on glycine[11] have indicated that the ballistic electron may resonantly react with that species prior to their thermalized solvation and that such resonant intermediates are responsible for the dissociative stabilization processes which occur during the reactive molecular breakup, thereby disrupting the chemistry of any cellular components.

The present study is organized as follows: the next section outlines our computational modeling, and section III reports our results for the glycine molecule, analyzing in detail the structures of our computed TNIs in section IV. Section V reports our conclusions and summarizes the present findings.

II. Theoretical Framework

Within the Born−Oppenheimer (BO) approximation one represents the total wave function of the $(N + 1)$ electrons when an electron scatters from an N-electron molecular target as an antisymmetrized product of electronic wave functions that parametrically depend on the nuclear coordinates. Since the present treatment of the scattering process is limited to an analysis of the elastic channels, no excitations will be considered for either the bound electrons or the bound nuclei. The description of the bound electron wave function will be given as a single-determinant of near-Hartree−Fock molecular orbitals (MOs) describing the N-bound electrons. To obtain our scattering equations, we then expand both the bound MOs and the continuum electron in a single-center expansion (SCE) around the center of mass of the target by employing symmetry-adapted angular functions. If one then expands the scattering state as the product of a one-electron scattering function and a single determinant target wave function, one obtains the static exchange representation of the electron−molecule interaction for the ground state. Additionally, to reduce the computational task, we have replaced the exact nonlocal exchange interaction with an energy-dependent local exchange potential[25]

$$V_{\mathrm{ex}}^{\mathrm{FEGE}}(\mathbf{r}) = \frac{2}{\pi} k_{\mathrm{F}}(\mathbf{r}) \left(\frac{1}{2} + \frac{1-\eta^2}{4\eta} \ln \left| \frac{1+\eta}{1-\eta} \right| \right) \qquad (1)$$

where $\eta(\mathbf{r}) = (k^2 + 2I_{\mathrm{p}} + k_{\mathrm{F}}(\mathbf{r}))^{1/2}/k_{\mathrm{F}}(\mathbf{r})$, $k_{\mathrm{F}}(\mathbf{r}) = (3\pi^2\rho(\mathbf{r}))^{1/3}$ is the local Fermi momentum, and I_{p} is the ionization potential of the molecular target.

In the present approach we include the effects from dynamical short-range correlation through the addition of a local energy-independent potential V_{corr}.[25,26] The V_{corr} is obtained by defining an average dynamical correlation energy of a single electron within the formalism of the Kohn and Sham variational scheme (for details, see also refs 26 and 27). The functional derivative of such a quantity with respect to the SCF N-electron density of the molecular target provides a density functional description of the required short-range correlation term, this being an analytic function of the target ground-state electron density. When studying the full scattering problem, we usually correct the large r behavior of V_{corr} so that it agrees with the known static polarizability of the target molecule.[18] However, in the present study we are only studying the resonant states, which are confined to the region of the molecule and are thus not markedly affected by the incorrect large r behavior of V_{corr} used in the present calculations. In other words, to correctly generate the full interaction within 12 Å from the molecular center of mass is sufficient to realistically describe the "localized" scattering states which give rise to TNI species.

To examine in some detail the mechanism and qualitative characteristics of low-energy, one-electron resonances requires a model which is simple enough to be computationally attractive but with sufficient details of the full scattering problem to reproduce the essential features of the realistic cases.[11] To facilitate the analysis of scattering resonances, we have used an adiabatic representation of the electron−molecule interaction potential. We start by noting that the standard, symmetry-adapted angular momentum eigenstates do not form the most compact angular set for the electron−molecule scattering problem: an alternative expansion basis is provided by diagonalizing the angular Hamiltonian at each radius r. These new angular eigenstates are the adiabatic angular functions which are distance-dependent, linear combinations of the symmetry-adapted "asymptotic" harmonics. The eigenvalues of the angular Hamiltonian then form an adiabatic radial potential over the selected range of the e^-−molecule distance.

To avoid the nonadiabatic coupling terms, we employ a piecewise diabatic (PD) representation for the potential[17−19] where the radial coordinate is divided into several regions so that sector i is defined as $r_{i-1} < r < r_i$, with $r_0 = 0$. In each region we average the coupling potential over r, and the resulting averaged potential is diagonalized to yield a set of angular functions. Then in region i the scattering potential is transformed into the new representation in which it is nearly diagonal. To solve the radial equations using this approach requires matching of the radial functions and their derivatives at the boundary between radial regions. The scattering was then solved within the reduced basis of the effective diabatic potential terms, and the corresponding poles of the **S** matrix have been obtained in the energy range of experimental interest, i.e., from threshold to about 15 eV.

III. Computed Transient Negative Ions (TNIs)

To obtain the resonant states the poles of the **S**-matrix were computed using 90 radial regions including PD potential terms up to $l = 9$ (including 55 radial functions for the A′ symmetry component and 45 for the A″ symmetry component, within the C_s symmetry of the target molecule). The bound target electrons were computed at the 6-31G(D) quality of basis set expansion,[8] and three different optimized geometries were considered since they were those located very close in energy to each other as obtained from the above calculations (typical $\Delta E \sim 7$ kJ mol^{-1}).[8]

The mapping of the A′ resonant states was done in the plane of the molecule, while the A″ TNI states have been mapped in a plane which is located at 0.75 au above the molecular plane since these are π states which have a nodal surface in the plane of the molecule. The calculations of the potential were carried out up to $l_{\mathrm{max}} = 80$ for its initial multipolar expansion, while the scattering wave functions included partial waves up to $l_{\mathrm{max}} = 40$. The V_{corr} was obtained from the DFT formulation discussed above and using the results of ref 19. The radial integration was carried out up to $r_{\mathrm{max}} = 12$ au, whereby the energy locations and widths of our resonant states were deemed to be numerically converged to within 10% of their converged value.

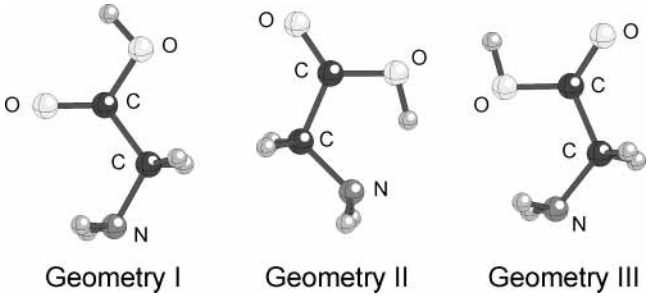

Figure 1. 3D geometries of the lowest energy configurations of glycine considered in this work. All geometries were obtained by global optimization.[8] The unlabeled atoms are H atoms.

TABLE 1: Computed Energy Positions and Widths (Both in electronvolts) of All the Metastable Anionic States of Glycine Found in the Present Work (Numbering of Geometries Corresponds to That of Figure 1)

symmetry	geometry	ER (eV)	GR (eV)
A″	I	3.14	0.23
	II	3.37	0.37
	III	2.98	0.26
A′	I	8.59	0.77
		8.73	3.82
		11.99	1.94
	II	7.47	1.68
		9.46	1.29
		13.00	1.96
	III	8.26	1.67
		8.86	1.24
		12.48	1.92

The structure of the piecewise diabatic model potential curves is shown, as an example for the A′ symmetry, in the lower panel of Figure 2.

One clearly sees there the presence of strongly coupled diabatic potentials and the location of several crossings at radial regions corresponding to the position of the molecular nuclei in one of our chosen minimum geometries (glycine I, see Figure 1): the distances are taken from the molecular center of mass. We also see there that with l_{max} up to 5 we are essentially describing the inner molecular region sampled by the scattered electron, although we kept in the calculations the potential curves with l_{max} up to 9, to ensure numerical convergence of our resonance features.

The upper panel of the same Figure 2 shows our results for the computed poles of the **S**-matrix represented on the complex energy plane, for the range of real parts of the energies from threshold to 15 eV: the calculations refer to one symmetry, the A′ irreducible representation (IR), and to one of the three geometries we have examined. One sees that only three of the resonances obtained show widths (imaginary energy values) smaller than their energy location: they are the ones that could be considered as describing resonances that lead to a time delay in the scattering at real energies. The locations and widths of all the resonances are given in Table 1.

A quick perusal of the data in that table shows marked similarities between the resonances produced by the three different geometries, thus suggesting that all the resonances are likely to be present for any choice of structure from the three most stable structures and therefore can be seen as being features of the glycine system rather than of any special geometry chosen for it. Furthermore, we see that the one located lowest in energy corresponds to a single resonance of A″ symmetry, i.e., one possessing a node on the molecular plane of highest symmetry, while the A′ symmetry supports three different TNI states which are located over a broad range of energies above threshold. We

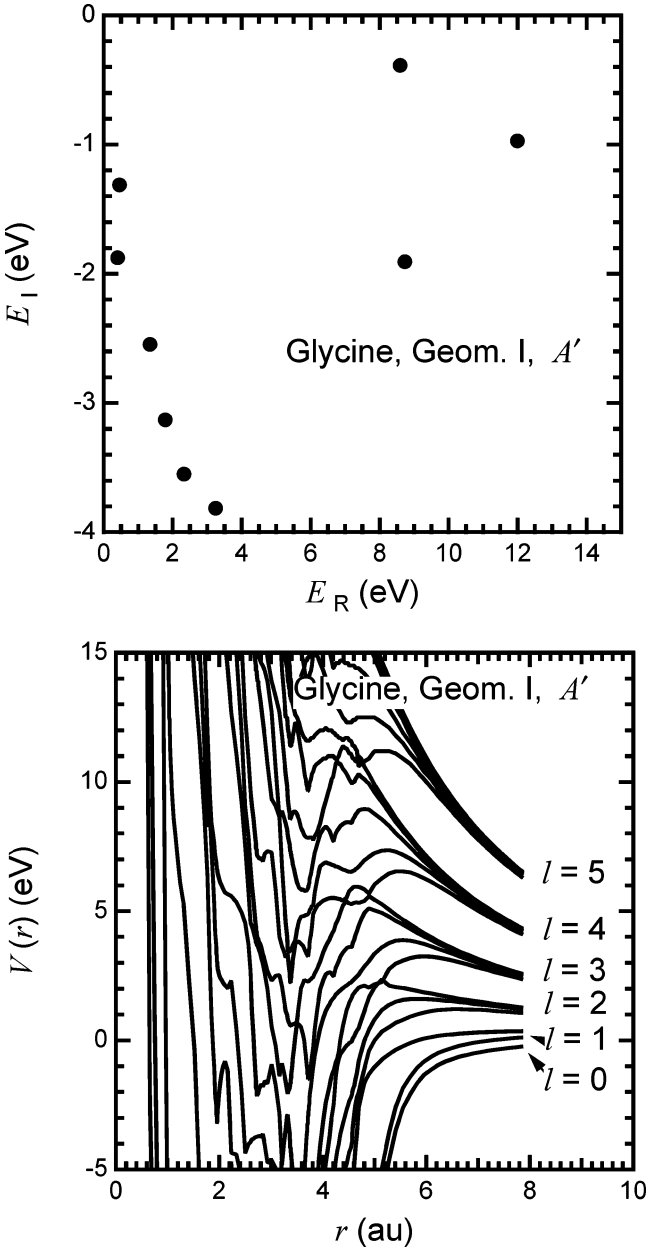

Figure 2. Upper panel: positions and widths in the complex energy plane of the computed resonances of A′ symmetry for the glycine molecular geometry I of the previous figure. Lower panel: Piecewise diabatic (PD) potential curves for the lower contributing angular momenta in the A′ symmetry for the same glycine geometry as that above.

have therefore produced spatial maps of the TNI states described by the above resonances in order to see if their spatial features allow us to make a connection with the DEA fragmentation channels experimentally observed for this molecule in recent gas-phase measurements.[11]

IV. Spatial Mapping of Resonant Electrons

The wave functions that describe resonant states correspond, in the case of shape resonances, to metastable electron states which are more localized than any of the scattering states close to them in energy. Thus, it becomes useful, to get some feeling on the physical consequences of this localization, to examine the resonant wave functions and to try to relate them, if possible, with specific direct fragmentation patterns experimentally observed in DEA processes.[11]

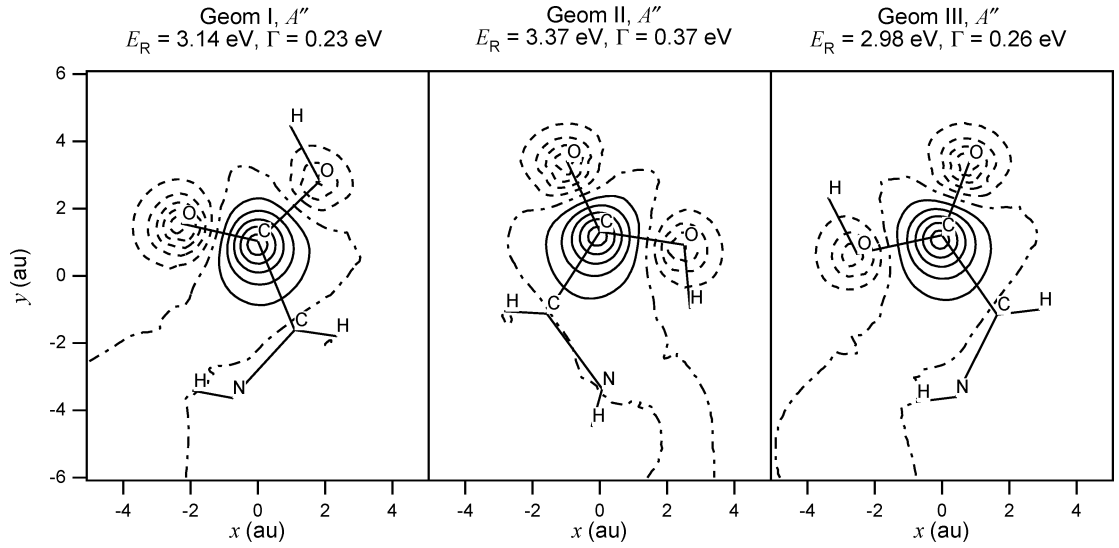

Figure 3. Resonant wave functions of A″ symmetry found for the three glycine configurations shown in Figure 1. The solid and dashed lines correspond to positive and negative values of the resonant wave functions. The dotted−dashed lines correspond to nodes in the wave functions. For each resonant electron the position and width are given in electronvolts. The wave functions are plotted at 0.75 au above the plane of the molecule.

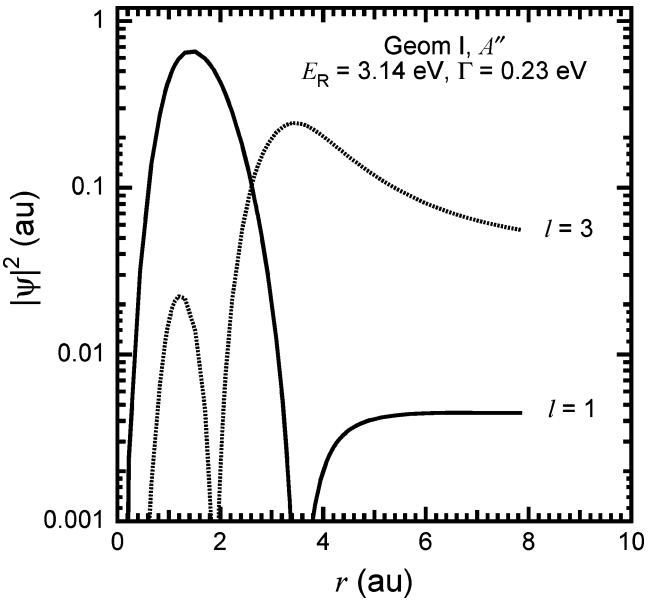

Figure 4. Dominant partial-wave contributions (of the radial distribution functions) for the radial components of the resonant electron of A″ symmetry associated with the density map of Figure 3 and for the geometry I of glycine.

The three panels of Figure 3 show projections on a plane containing the molecular backbone of the wave function, associated with the lowest resonant state (of A″ symmetry) obtained from our calculations. The energy position of this resonant state is given for the three configurations around 3 eV and with a width averaged over the three configurations of about 0.3 eV. The corresponding radial components of the wave function for the same three molecular geometries are given in Figure 4.

The present results of a narrow resonance in the low-energy region can be related to what has been experimentally found from electron-impact experiments on gas-phase glycine.[11] It was reported there, in fact, that two distinct fragmentation peaks appear in the 2−3 eV region: (i) one peak centered around 1.4 eV that yielded $[Gly-H]^-$ ions, i.e., negative ions with one H atom missing from the molecule, and (ii) another, broader peak centered around 2 eV and associated with a negative ion with NH_3/OH detachment, i.e., to either the $CHCOOH^-$ or to the $H_2NCH_2CO^-$ negative ion fragments. Because of the approximations involved in our model calculations, we cannot expect the position of our computed resonance to exactly match the above observations, but we certainly find that our A″ resonance, given by all three geometries considered, is located between 2.7 and 3.4 eV, with an average width of about 0.3 eV.

The excess electron is chiefly localized on the main molecular backbone, without any residual charge on the H atoms of the $-NH_2$, $-CH_2$, or $-OH$ groups. It therefore seems possible that the subsequent DEA process will stabilize a molecular anion with the loss of an H atom leading to the $[Gly-H]^-$ ion formation.

The excess electron of the resonant state is being chiefly trapped behind the $l = 3$ barrier, as shown as an example in Figure 4 for the I configuration, and presents several marked nodal planes.

In all three configurations of Figure 3 one sees that a nodal plane crosses the C−OH bond but not the $C-NH_2$ bond, i.e., that the former bond can take up antibonding character from the additional electron density stabilized by the resonant process, while the latter bond is not modified in the same way. The present resonance could therefore also be considered a precursor state that leads to excess electron stabilization on the $H_2NCH_2CO^-$ fragment with elimination, via a DEA mechanism, of the $-OH$ group.

We also note that, as in the experiments, we do not find here any resonance near threshold, of either A′ or A″ symmetry, which could be construed as leading to excess electron density being localized on the H atom, thereby creating a possible precursor state for H^- detachment. The experiments, in fact, did see an H^- signal at threshold, but this was attributed to experimental artifacts inherent to 0 eV DEA detection.[11] Thus, the lack of believable H^- signal in the experiments[12] is matched by the absence in our calculations of a possible precursor state for it.

To make our analysis pictorially clearer in Figure 4, we report the dominant angular momenta (partial waves) that contribute to the resonant electron wave function mapped in the previous Figure 3. One clearly sees that the scattered electron forming the metastable state is chiefly described by its $l = 3$ component

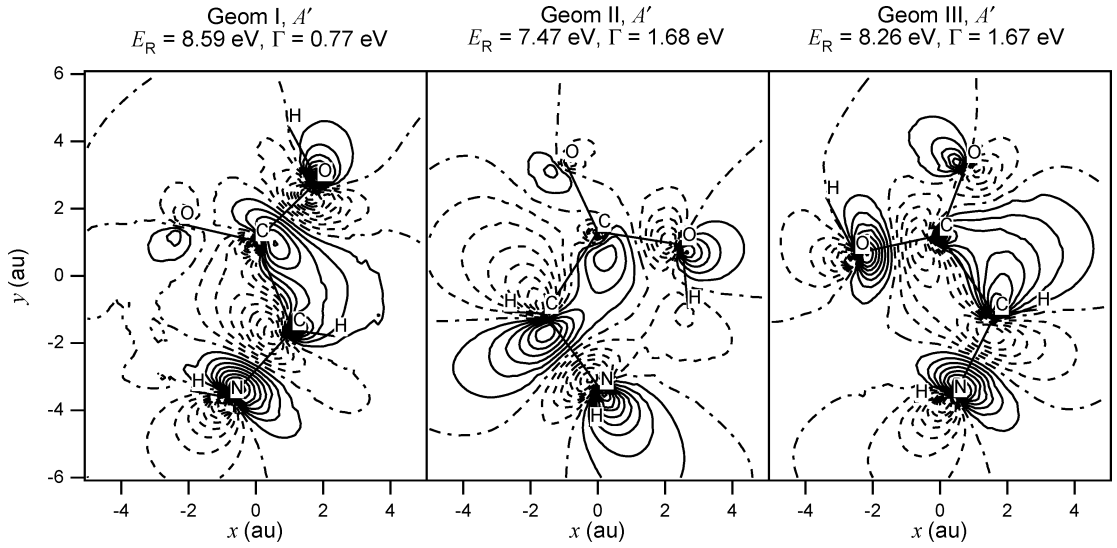

Figure 5. Lowest energy resonant wave function of A′ symmetry for the three glycine configurations shown in Figure 1. The solid and dashed lines correspond to the positive and negative values of the resonant wave functions. The dotted−dashed lines correspond to nodes in the wave functions. The wave functions are plotted in the plane of the molecule.

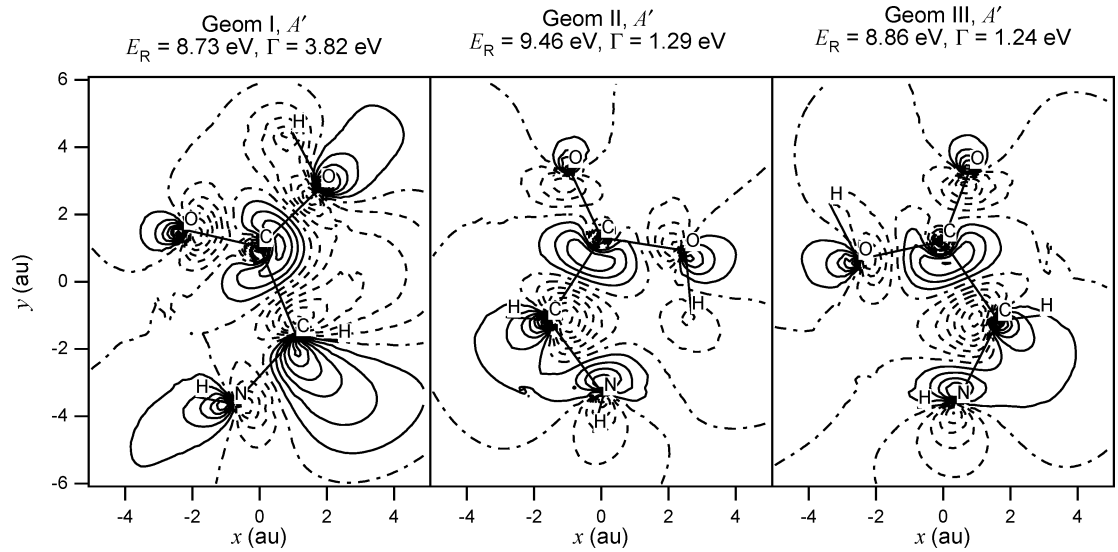

Figure 6. Same as in Figure 5 but for the next resonance of A′ symmetry at higher energies with respect to those of Figure 5. The notation remains the same as in that figure.

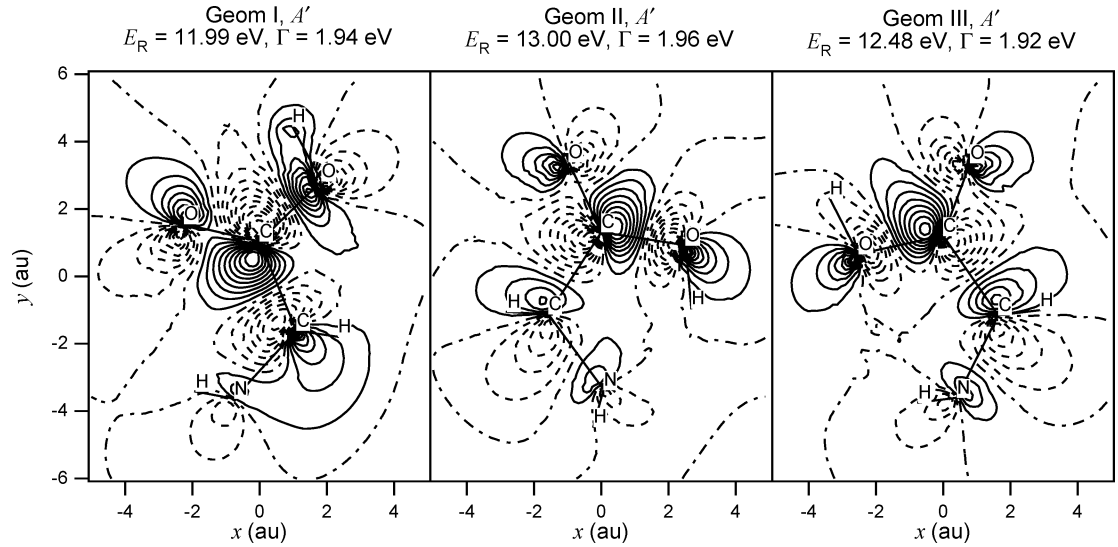

Figure 7. Same as in Figure 5 but for the third resonance of A′ symmetry, located at the highest energy within the range examined in this work. The notation remains the same as in the other figures.

on the periphery of the molecule. This indicates that the state is trapped by the $l = 3$ angular momentum barrier. The resonant wave functions shown in Figure 3 appear to be a typical C−O π^* orbital with some additional antibonding character between the C and the OH oxygen atom.

In the three panels reported in Figures 5 and 6 we show the computed TNI states of A′ symmetry that are positioned at higher energies; i.e., the first one (Figure 5) appears located, on average, above 8.0 eV, while the second resonant state (Figure 6) is located closer to 9.0 eV. The latter resonance also exhibits a larger average width (∼2.1 eV) than the former (∼1.4 eV).

The experimental DEA data[11] further indicate that at energies above the appearance of the three fragments described above, i.e., $[Gly-H]^-$, $[H_2C_2O_2^-]$, and $[H_4C_2NO]^-$, further fragmentation peaks are located in the region of energy between ∼6.0 and 8.0 eV, where other, smaller fragments are detected: O^-/NH_2^-, HO^-, CN^-, H_2CN^-, HCO_2^-, and $H_2C_2NO^-$. The experiments also report the presence of an intense and broad fragmentation signal for O^-/NH_2^-, centered around 12.0 eV.[11] It is thus of interest to see how the two TNI states obtained in our calculations of Figures 5 and 6 and located between 8 and 9 eV as broad resonances can be used to rationalize some of the experimental fragmentation patterns described above. The resonant electron wave functions of Figure 5 clearly show the presence of two nodal planes (signatures of antibonding character in the localized wave function) across the $C-NH_2$ bond and across the C−OH bond. They further show very little excess electron densities located over the terminal H atoms of either −OH or $-NH_2$ functional groups. It therefore seems reasonable to surmise that the fragmentation could occur by forming OH^- and NH_2^- fragments and that, in some of the DEA channels, the fragmentation process would extend to the formation of O^- fragments.

The resonance wave functions of Figure 6 indicate instead that the antibonding character of the resonant orbital is located across the central C−C. This suggests that the primary fragmentation of this TNI is via the breakup of that central bond of the molecular framework. The products of such a breakup would be fragments such as H_2CN^- or HCO_2^-, obtained by the two primary fragments (H_4CN and HCO_2) by electron attachment on either of them followed by H losses from the carbon atom of the former fragment and due again to the lack of excess electron density on such atoms (see Figure 6): these are indeed two prominent peaks of the fragmentation pattern experimentally observed, i.e., H_2CN^- and HCO_2^-. The former peak could also undergo H atom loss (as little charge is located on such atoms; see Figure 6), to give rise to CN^- fragments as experimentally observed. Finally, after −OH detachment with excess charge left on the residual main fragment, another possible decay route of the TNI state of Figure 6 (because of the additional nodal plane across the C−O bond) is with the larger fragment undergoing partial hydrogen abstraction processes with the formation of $(HN-CH-C=O)^-$, as experimentally observed. Thus, all observed fragments for glycine in the gas phase could be described as originating from the TNI states found in our calculations, states which can then follow different fragmentation routes and lead therefore to different final negative stable ions.

In the calculations reported in Figure 7 we also show the spatial maps of the resonance state that we found to appear at the highest energy position, i.e., around 12−13 eV. The width of this resonance also turns out to be one of the largest: an average value of about 1.94 eV. The analysis of its nodal structure indicates the antibonding character of the excess electron to be across the C−OH bond and the $C-NH_2$ bond. There is also another nodal plane across the central C−C bond, although without the strong density buildup on the C atoms observed in Figure 6. The appearance of experimental peaks for OH^-/NH_2^- fragments around 12.0 eV [11] could therefore be connected with the presence of this resonant orbital that would undergo dissociative losses of the above ions at an energy higher than that of the lower resonance of Figure 5 discussed above in the context of other experimental peaks.

V. Summary and Conclusions

A fuller theoretical description of the above DEA mechanisms at the molecular level requires establishing first the structures and the locations of the resonant intermediates, followed by the dynamical description of their stabilization into the different fragmentation channels that lead to different final anions. In our present treatment we have focused our analysis on the initial step of the e^-−molecule dynamics and have tried to extract from quantum scattering calculations, using a model nonempirical interaction potential to solve the coupled channel equations, the energy locations, the widths, and the structural properties of the intermediate metastable states. In our analysis such intermediate, resonant complexes are taken to be formed first as single-particle, open-channel resonances due to angular-momentum barrier trapping and thus we have not included in our model any provision for Feshbach-type two-electron resonances. The latter resonances are also very likely to occur and to lead to core-excited shape-resonance trappings coupled to our single-channel mechanisms. Our analysis has not included the multidimensional nuclear dynamics necessary to follow the various DEA processes, another computational extension that is not yet possible for glycine using present-day computational tools. However, it is certainly suggestive that the four different resonant states identified by our calculations can be related to the nine fragmentation channels experimentally observed. The antibonding features revealed by the nodal characteristics of the resonant wave functions obtained here can rationalize, albeit qualitatively, possible fragmentation patterns and can indicate our TNI structures as likely to be the precursor states for the final DEA species observed in the gas phase.

Acknowledgment. We are grateful to the Italian Ministry for Research (MUIR), to the Research Committee of the University of Rome "La Sapienza", to the NATO program for collaborative research grants, to the Welch Foundation for support under grant A-1020, and to the European V Framework through the EPIC project for their financial support. We are also grateful to Leon Sanche and to Eugen Illenberger for several stimulating discussions and for making us aware of this very interesting area of research.

References and Notes

(1) Schaefer, L.; Sellers, H. L.; Lovas F. J.; Suenram, R. D. *J. Am. Chem. Soc.* **1980**, *102*, 6566.
(2) Suenram, R. D.; Lovas, F. J. *J. Am. Chem. Soc.* **1980**, *102*, 7180.
(3) Brown, R. D.; Godfrey, P. D.; Storey, J. W. V.; Bassez, M. P. *J. Chem. Soc., Chem. Commun.* **1978**, 547.
(4) Cannington, P. H.; Ham, N. S. *J. Electron Spectrosc. Relat. Phenom.* **1983**, *32*, 139.
(5) Shipman, L. L.; Christoffersen, R. E. *Theor. Chim. Acta* **1973**, *31*, 75.
(6) Tse, Y.-C.; Newton, M. D.; Vishveshwara, S.; Pople, J. A. *J. Am. Chem. Soc.* **1978**, *100*, 4329.
(7) Jensen, J. H.; Gordon, M. S. *J. Am. Chem. Soc.* **1991**, *113*, 7917.
(8) Aflatooni, K.; Hitt, B.; Gallup, G. A.; Burrow, P. D. *J. Chem. Phys.* **2001**, *115*, 6489.

(9) O'Hair, R. A. J.; Blanksby, S.; Styles, M.; Bowie, J. H. *Int. J. Mass Spectrom.* **1999**, *182*−*183*, 203.

(10) Gutowski, M.; Skurski, P.; Simons, J. *J. Am. Chem. Soc.* **2000**, *122*, 10159.

(11) Gohlke, S.; Rosa, A.; Illenberger, E.; Brüning, F.; Huels, M. A. *J. Chem. Phys.* **2002**, *116*, 10164.

(12) Ptasinka, S.; Denifl, S.; Abedi, A.; Scheier, P.; Märk, T. D. *Anal. Bioanal. Chem.* **2003**, *377*, 1115.

(13) Boudaïffa, B.; Cloutier, P.; Hunting, D.; Huels, M. A.; Sanche, L. *Science* **2000**, *287*, 1658.

(14) Huels, M. A.; Boudaïffa, B.; Cloutier, P.; Hunting, D.; Sanche, L. *J. Am. Chem. Soc.* **2003**, *125*, 4467.

(15) Barrios, R.; Skurski, P.; Simons, J. *J. Phys. Chem. B* **2002**, *106*, 7991.

(16) For a comprehensive review, e.g., see: Gianturco, F. A., Huo, W. M., Eds. *Computational Methods for Electron*−*Molecule Collisions*; Plenum: New York, 1995.

(17) Gianturco, F. A.; Lucchese, R. R.; Sanna, N. *J. Phys. B: At., Mol. Opt. Phys.* **1999**, *32*, 2181.

(18) Gianturco, F. A.; Lucchese, R. R. *J. Chem. Phys.* **1999**, *111*, 6769.

(19) Lucchese, R. R.; Gianturco, F. A. *Int. Rev. Phys. Chem.* **1996**, *15*, 429.

(20) Gianturco, F. A.; Kashenock, Yu. G.; Lucchese, R. R.; Sanna, N. *J. Chem. Phys.* **2002**, *116*, 2811.

(21) Gianturco, F. A.; Lucchese, R. R. *J. Chem. Phys.* **2003**, *120*, 7446.

(22) Hanel, G.; Gstir, B.; Denifl, S.; Scheier, P.; Probst, M.; Farizon, B.; Farizon, M.; Illenberger, E.; Märk, T. D. *Phys. Rev. Lett.* **2003**, *90*, 188104.

(23) For an extensive review see: Sanche, L. *Mass Spectrosc. Rev.* **2002**, *21*, 349.

(24) E.g. see: Aldrich, J. E.; Lam, K. Y.; Shragge, P. C.; Hunt, J. W. *Radiat. Res.* **1975**, *63*, 42.

(25) Hara, S. J. *J. Phys. Soc. Jpn.* **1967**, *22*, 710.

(26) Perdew, J. P.; Zunger, A. *Phys. Rev. B* **1981**, *23*, 5048.

(27) Lee, C.; Yang, W.; Parr, R. G. *Phys. Rev. B* **1988**, *37*, 785.